ACS APPLIED ENERGY MATERIALS

www.acsaem.org Article

Efficient Solar Steam Generation of Carbon Black Incorporated Hyper-Cross-Linked Polymer Composites

Chaohu Xiao, Weidong Liang,* Qi-Meige Hasi, Fei Wang, Lihua Chen, Jingxian He, Fang Liu, Hanxue Sun, Zhaoqi Zhu, and An Li*

Cite This: *ACS Appl. Energy Mater.* 2020, 3, 11350−11358 Read Online

ACCESS | Metrics & More | Article Recommendations | Supporting Information

ABSTRACT: The creation of porous photothermal materials with high solar absorption and conversion efficiency is essential for the fabrication of efficient solar-driven interfacial evaporation devices. Herein, we demonstrate a strategy for scalable fabrication of solar steam generators based on hyper-cross-linked polymers (HCPs) in situ doped with carbon black (named C-[BzMim]Cl-*co*-PhH and C-[BzPy]Br-*co*-PhH). The monolithic HCPs composites consist of a hyper-cross-linked polymer skeleton and randomly distributed carbon black particles, which take advantage of both highly abundant porosity of HCPs and excellent light absorption of carbon black to create solar steam generators in a facile one-step preparation. By combining with their good thermal insulation (C-[BzMim]Cl-*co*-PhH 0.168 W m^{-1} K^{-1} and C-[BzPy]Br-*co*-PhH 0.123 W m^{-1} K^{-1}) in wet conditions, the HCPs composites show high photothermal conversion performance with efficiencies of 85.2% and 88.4% for C-[BzMim]Cl-*co*-PhH and C-[BzPy]Br-*co*-PhH under 1 sun illumination, respectively. Moreover, the HCPs composites also exhibit excellent salt-resistance performance in solar steam generation (SSG), and the purified water can be used as domestic water. On the basis of such a simple and scalable fabrication approach as well as desired SSG performance, it is suggested that the HCPs composites may have great potentials as promising solar steam generators for real applications.

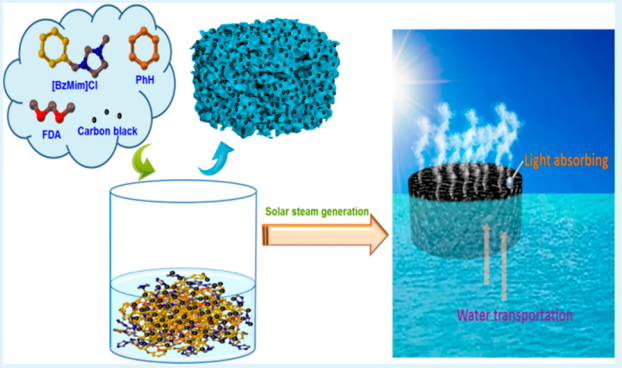

KEYWORDS: *solar steam generation, photothermal materials, hyper-cross-linked polymers composites, one-step preparation, salt resistance*

1. INTRODUCTION

The severe energy crisis and clean water scarcity have been growing challenges worldwide because of the development of modern industry and a rapidly growing population.[1−3] Various desalination strategies have been applied to address these issues, such as nanofiltration, ion exchange, and RO; however, huge energy consumption usually accompanies these strategies.[4,5] SSG is emerging as one of the promising technologies for desalination, as it harvests renewable solar energy and localized the solar irradiation onto the upper surface of photothermal materials to maximum convert it into steam energy.[6−8] Based on such a unique vaporization manner, SSG devices always show high energy conversion efficiency. As a result, extensive attention has been given to explore new photothermal materials for construction of an efficient SSG system for fresh water production.[9−11]

In general, ideal photothermal materials should have characteristics of porous structure, excellent light absorption, and good thermal insulation.[12−16] Up to now, various kinds of photothermal materials, including carbon materials,[17−20] biomass materials,[21−23] organic materials,[24−27] polymers,[28−30] and hydrogels,[31−35] have been developed according to this design principle. Among these mentioned investigations, porous organic polymer (POP) based photothermal materials have recently received considerable attention due to their adjustable porosity, excellent physical−chemical stability, and controllable preparation.[36−38] Until now, POP based photothermal materials such as conjugated microporous polymers (CMPs) and phenolic aldehyde foams (PAFs) have been created.[39−41] Compared to those traditional porous photothermal materials usually with unadjustable porosity, the POPs have intrinsic porous features, and their porosity could be tailored by rational selecting different building blocks with various molecular sizes and thus have great advantages for tailor-design of functional photothermal materials with the desired porosity.

Received: September 16, 2020
Accepted: October 19, 2020
Published: October 28, 2020

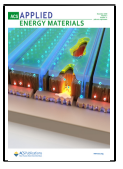

In this work, quite different from the recently reported strategies on creation of polymer-based solar generators, we demonstrate the fabrication of photothermal materials based on hyper-cross-linked polymer (HCP) composites which were synthesized by using [BzMim]Cl, [BzPy]Br, and benzene as building blocks by Friedel−Crafts alkylation reaction in the presence of carbon black. The merits of our materials are as follows: (1) As a kind of subclass of POPs, HCPs normally use low-cost and bulk chemicals such as benzene or other common aromatics as building blocks with inexpensive catalysts (i.e., $FeCl_3$). Therefore, HCP based photothermal materials are generally cheap and readily available. (2) Compared with those double-layered POP based photothermal materials usually need to coat light-absorbing materials to enhance their light absorption; our HCP composites benefit from both the porous feature of HCPs and the superior light-absorbing ability of in situ doped carbon black and thus avoid construction of double-layered structure. Therefore, such integrated HCP composites have advantages of simple one-step fabrication. As a proof-of-concept study, the resulting HCP composites exhibit high evaporation efficiencies of 85.2% and 88.4% for C-[BzMim]Cl-*co*-PhH and C-[BzPy]Br-*co*-PhH under 1 sun illumination. To our knowledge, such photothermal materials based on HCPs composites have never been reported so far. The one-step fabrication strategy obtained from this study, however, may offer new opportunities for the rational design and fabrication of composite photothermal materials for solar-driven interfacial evaporation.

2. EXPERIMENTAL SECTION

2.1. Materials. 1-Benzyl-3-methylimidazolium chloride ([BzMim]Cl) was obtained from Lanzhou Zhongke Kaiteke Industry and Trade Co., Ltd. *N*-Benzylpyridinium bromide ([BzPy]Br) was obtained from Shanghai Chengjie Chemical Co., Ltd. Benzene (PhH) was provide by Yantai Shuangshuang Chemical Co., Ltd. Formaldehyde dimethyl acetal (FDA) was obtained from J &K Chemical Ltd. 1,2-Dichloroethane (DCE) was obtained from Tianjin Damao Chemical Reagent Factory. Anhydrous ferric chloride ($FeCl_3$) and carbon black were purchased from Shanghai Macklin Biochemical Co., Ltd. Methanol was obtained from Sinopharm Chemical Reagent Co., Ltd. All chemicals were used as received without additional purification.

2.2. Preparation of the C-[BzMim]Cl-*co*-PhH and C-[BzPy]Br-*co*-PhH. In a typical synthesis, 1-benzyl-3-methylimidazolium chloride ([BzMim]Cl, 0.63 g), benzene (PhH, 0.47 g), and formaldehyde dimethyl acetal (FDA, 0.69 g) were dissolved in 20.0 mL of 1,2-dichloroethane (DCE). After the ionic liquids completely dissolved, anhydrous ferric chloride ($FeCl_3$, 1.95 g) and carbon black (0.5 g) were added under the protection of nitrogen. The above mixed solution was stirred for 1 h at room temperature and then treated at 75 °C for 24 h. The HCPs were obtained as black cylinders, soaked in methanol to remove impurities, and then the solvent was replaced with distilled water to obtain the C-[BzMim]Cl-*co*-PhH. The C-[BzPy]Br-*co*-PhH was obtained the same as C-[BzMim]Cl-*co*-PhH, except *N*-benzylpyridinium bromide ([BzPy]Br) was used as one of the monomers.

3. RESULTS AND DISCUSSION

The HCPs were prepared via facile Friedel−Crafts alkylation, and the synthesis process is shown in Figure 1a. The HCPs were synthesized by using 1-benzyl-3-methylimidazolium chloride ([BzMim]Cl), *N*-benzylpyridinium bromide ([BzPy]-Br), and benzene as monomers, formaldehyde dimethyl acetal (FDA) as cross-linker, 1,2-dichloroethane (DCE) as solvent, a moderate amount of carbon black, and promoted by

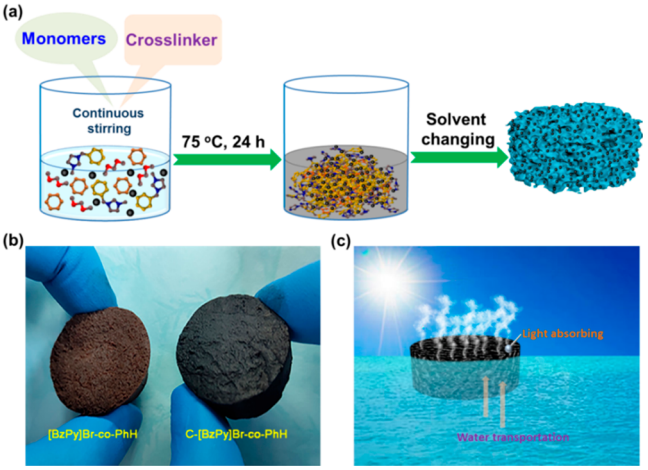

Figure 1. (a) Synthesis process of C-[BzMim]Cl-*co*-PhH and C-[BzPy]Br-*co*-PhH. (b) Photos of [BzPy]Br-*co*-PhH and C-[BzPy]Br-*co*-PhH. (c) Schematic of the C-[BzMim]Cl-*co*-PhH and C-[BzPy]Br-*co*-PhH solar steam generations.

anhydrous ferric chloride ($FeCl_3$). The mixture was heated at 75 °C for 24 h under the protection of nitrogen; the HCPs were obtained as black cylinders and then soaked in methanol and distilled water alternately to obtain the HCPs. The monolithic HCPs prepared through the simple synthesis strategy are shown in Figure 1b; the [BzPy]Br-*co*-PhH appears dark brown and turns to black with the addition of carbon black. As shown in Figure 1c, by use of such a strategy the prepared C-[BzMim]Cl-*co*-PhH and C-[BzPy]Br-*co*-PhH can harvest light and serve as efficient solar steam generators directly.

The surface chemical compositions of the C-[BzMim]Cl-*co*-PhH and C-[BzPy]Br-*co*-PhH were characterized by XPS analysis. As shown in Figure 2a, the full XPS spectra of C-[BzMim]Cl-*co*-PhH including characteristic peaks of C 1s (284.1 eV), N 1s (400.1 eV), O 1s (531.1 eV), and Cl 2p (200.1 eV), indicating that the chemical components of the C-[BzMim]Cl-*co*-PhH are carbon, nitrogen, oxygen, and chlorine.[42,43] The C 1s spectra of C-[BzMim]Cl-*co*-PhH can be distinguished into three subpeaks (Figure 2b), including C−C (284.6 eV), aromatic C−C (285.3 eV), and C−N/C═N (286.2 eV).[44−46] Compared to C-[BzMim]Cl-*co*-PhH, the characteristic peaks of Br 3d (67.1 eV) can be observed clearly in the full XPS spectra of C-[BzPy]Br-*co*-PhH (Figure 2c). The C 1s spectra of C-[BzPy]Br-*co*-PhH also can be distinguished into three subpeaks (Figure 2d), including C−C (284.6 eV), aromatic C−C (285.3 eV), and C−N/C═N (286.2 eV).[44−46] All of the above XPS analysis confirmed that the C-[BzMim]Cl-*co*-PhH and C-[BzPy]Br-*co*-PhH were synthesized successfully.

The morphologies of the C-[BzMim]Cl-*co*-PhH and C-[BzPy]Br-*co*-PhH were characterized by scanning electron microscopy (SEM). As shown in Figure 3a,b,g,h, the SEM images show that plenty of irregular particles attached on the hyper-cross-linked polymer skeletons to form the C-[BzMim]-Cl-*co*-PhH and C-[BzPy]Br-*co*-PhH and then built a three-dimensional porous structure. The porous C-[BzMim]Cl-*co*-PhH and C-[BzPy]Br-*co*-PhH with carbon black particles embedded in the process of hyper-cross-linking possess good water transmission channels, while also exhibiting excellent light absorption. Therefore, the C-[BzMim]Cl-*co*-PhH and C-

https://dx.doi.org/10.1021/acsaem.0c02290
ACS Appl. Energy Mater. 2020, 3, 11350−11358

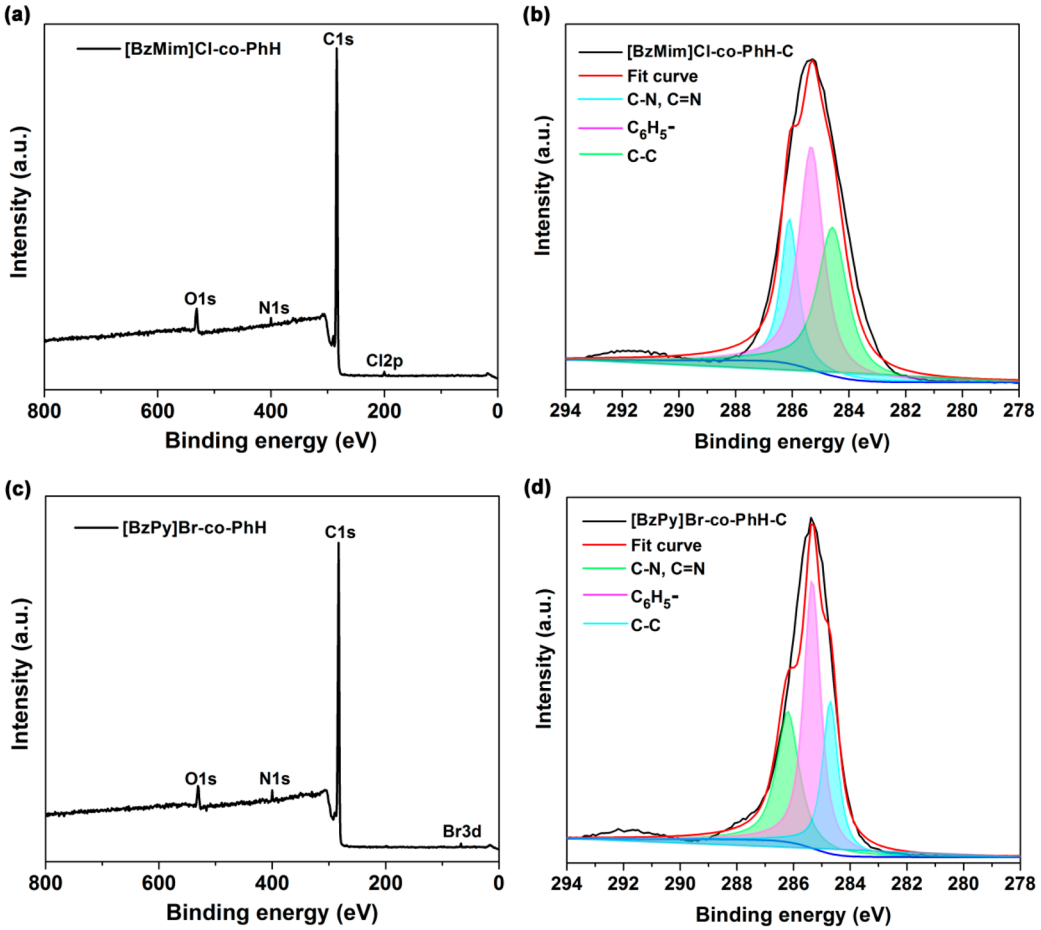

Figure 2. (a) Full XPS spectra of C-[BzMim]Cl-*co*-PhH. (b) C 1s XPS spectra of the C-[BzMim]Cl-*co*-PhH. (c) Full XPS spectra of C-[BzPy]Br-*co*-PhH. (d) C 1s XPS spectra of the C-[BzPy]Br-*co*-PhH.

[BzPy]Br-*co*-PhH can serve as promising solar steam generations directly. The EDS mapping of C-[BzMim]Cl-*co*-PhH and C-[BzPy]Br-*co*-PhH are depicted in Figure 3c–f,i–l, the uniform distributed C, N, O, and Cl elements can be clearly observed in C-[BzMim]Cl-*co*-PhH, while the uniform distributed C, N, O, and Br elements can be clearly observed in C-[BzPy]Br-*co*-PhH, and the EDS mapping analysis is consistent with the full XPS spectra mentioned above.

Powder X-ray diffraction (XRD) patterns of the C-[BzMim]Cl-*co*-PhH and C-[BzPy]Br-*co*-PhH show broad peaks located at 21.6° (Figure 4a), indicating the amorphous characters of C-[BzMim]Cl-*co*-PhH and C-[BzPy]Br-*co*-PhH are similar to the previously reported polymers.[47,40] The light absorption capability of the C-[BzMim]Cl-*co*-PhH and C-[BzPy]Br-*co*-PhH were investigated from the range 200–2500 nm by UV–vis–NIR spectrometry. As shown in Figure 4b, because of the addition of carbon black particles in the synthesis process, the resulting black C-[BzMim]Cl-*co*-PhH and C-[BzPy]Br-*co*-PhH exhibit almost 94% light absorption. Such excellent light absorption performance indicate that the C-[BzMim]Cl-*co*-PhH and C-[BzPy]Br-*co*-PhH can serve as desirable absorbers to harvest solar energy for solar-driven interfacial evaporation. The porosity properties of C-[BzMim]-Cl-*co*-PhH and C-[BzPy]Br-*co*-PhH were evaluated by nitrogen gas adsorption/desorption measurements. As depicted in Figure 4c, both C-[BzMim]Cl-*co*-PhH and C-[BzPy]Br-*co*-PhH are assigned to N_2 adsorption/desorption isotherms of type IV according to the IUPAC classification,[48] which indicate the C-[BzMim]Cl-*co*-PhH and C-[BzPy]Br-*co*-PhH mainly contain mesopores. The BET surface areas were found to be 583 m^2 g^{-1} for C-[BzMim]Cl-*co*-PhH and 489 m^2 g^{-1} for C-[BzPy]Br-*co*-PhH. The pore size distribution originated from the C-[BzMim]Cl-*co*-PhH and C-[BzPy]Br-*co*-PhH adsorption branches are calculated by the Barrett–Joyner–Hollander (BJH) method. As shown in Figure 4d, the pore size distribution mainly appears at 1.7–6.3 nm for C-[BzMim]Cl-*co*-PhH and 1.7–4.8 nm for C-[BzPy]Br-*co*-PhH, indicating the existence of micropores and mesopores in the C-[BzMim]Cl-*co*-PhH and C-[BzPy]Br-*co*-PhH.

The heat-insulated performance of C-[BzMim]Cl-*co*-PhH and C-[BzPy]Br-*co*-PhH were evaluated by using the flash method at room temperature. The thermal conductivity were measured to be 0.168 W m^{-1} K^{-1} for C-[BzMim]Cl-*co*-PhH and 0.123 W m^{-1} K^{-1} for C-[BzPy]Br-*co*-PhH in wet conditions; such low thermal conductivity can reduce the heat transfer to bulk water. To intuitively observe the heat-insulated performance of C-[BzMim]Cl-*co*-PhH and C-[BzPy]Br-*co*-PhH, an infrared camera was used to record the dynamic temperature changes of the bulk water under 1 sun irradiation, and infrared images were taken every 15 min to record the real-time temperature of middle of the water body. As shown in Figure 5, the temperature of the water body rise rapidly among the initial 30 min and slowly afterward. According to the record real-time temperature, the water body temperature of the C-[BzMim]Cl-*co*-PhH and C-[BzPy]Br-*co*-PhH devices rises to 25.6 and 25.0 °C within

https://dx.doi.org/10.1021/acsaem.0c02290
ACS Appl. Energy Mater. 2020, 3, 11350–11358

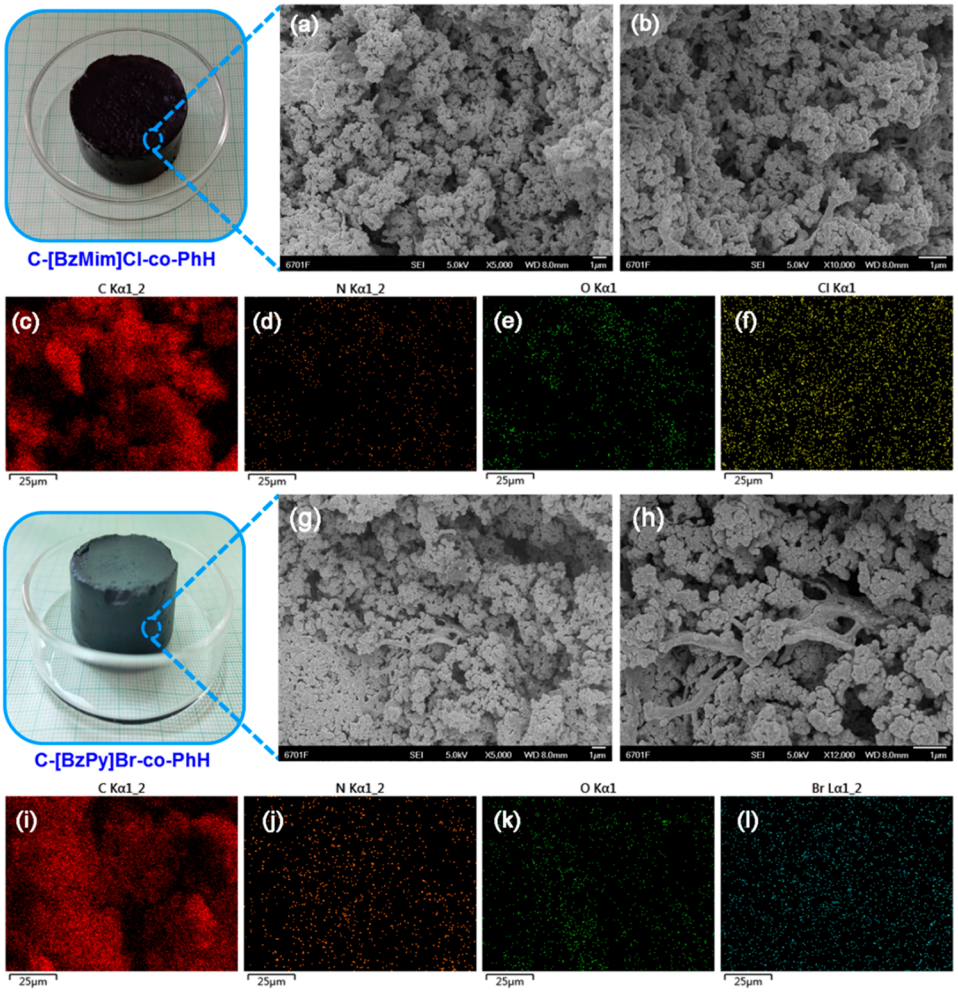

Figure 3. (a, b) SEM images of the C-[BzMim]Cl-*co*-PhH. (c–f) EDS mapping images of the C-[BzMim]Cl-*co*-PhH. (g, h) SEM images of the C-[BzPy]Br-*co*-PhH. (i–l) EDS mapping images of the C-[BzPy]Br-*co*-PhH.

the first 15 min and increases to 29.3 and 28.2 °C within 30 min under 1 sun illumination, respectively. Then the temperature reaches 32.3 and 31.2 °C within 60 min under 1 sun illumination, indicating the excellent heat-insulated performance of the C-[BzMim]Cl-*co*-PhH and C-[BzPy]Br-*co*-PhH.

The photothermal properties of the C-[BzMim]Cl-*co*-PhH and C-[BzPy]Br-*co*-PhH were investigated by using an infrared camera. The real-time surface temperature of C-[BzMim]Cl-*co*-PhH and C-[BzPy]Br-*co*-PhH under different illumination intensities are show in Figure 6a,b. It can be found that the surface temperatures of the C-[BzMim]Cl-*co*-PhH increase rapidly from room temperature to 39.8, 47.2, and 55.2 °C among the initial 30 min, and these values further reach up to 41.6, 47.7, and 56.2 °C under 1, 2, and 3 sun illumination intensities within 60 min, respectively. For C-[BzPy]Br-*co*-PhH the surface temperature rise to 40.5, 49.8, and 56.3 °C with the initial 30 min, and reach up to 42.4, 50.2, and 56.5 °C under 1, 2, and 3 sun illumination intensities within 60 min, respectively. Moreover, the detailed real-time surface temperatures are depicted in Figure 6c,d, the maximum surface temperatures are detected to be 41.6, 48.6, and 56.9 °C for C-[BzMim]Cl-*co*-PhH and 42.4, 50.2, and 57.5 °C for C-[BzPy]Br-*co*-PhH under 1, 2, and 3 sun irradiation, respectively. Duing to the addition of carbon black particles in the process of synthesis and excellent heat-insulated performance, the C-[BzMim]Cl-*co*-PhH and C-[BzPy]Br-*co*-PhH can absorb most of the sunlight and converted it into thermal energy.

To evaluate the solar energy conversion efficiency of C-[BzMim]Cl-*co*-PhH and C-[BzPy]Br-*co*-PhH, an electronic analytical balance was used to record the time-dependent mass changes of water resulting from water evaporation under different light power densities. As shown in Figure 7a,b, the amount of evaporated water increase as the intensity of the solar illuminations increase, and the evaporation rates are obtained from the slope of the time-dependent mass change curves. As depicted in Figure 7c,d, under 1, 2, and 3 sun illumination intensities, the evaporation rates of C-[BzMim]-Cl-*co*-PhH were calculated to be 1.36, 2.27, and 3.18 kg m^{-2} h^{-1}, and for C-[BzPy]Br-*co*-PhH these values are 1.43, 2.40, and 3.31 kg m^{-2} h^{-1}, respectively. As a control, the evaporation rate of pure water under 1 sun irradiation was measured and calculated to be 0.42 kg m^{-2} h^{-1}, which is much lower than that of C-[BzMim]Cl-*co*-PhH and C-[BzPy]Br-*co*-PhH at the same illumination intensity, indicating the C-[BzMim]Cl-*co*-PhH and C-[BzPy]Br-*co*-PhH possess good solar energy conversion performance. The energy conversion efficiency was calculated with reference to the reported literature,[49,50] and the detailed calculation procedures are presented in the

https://dx.doi.org/10.1021/acsaem.0c02290
ACS Appl. Energy Mater. 2020, 3, 11350–11358

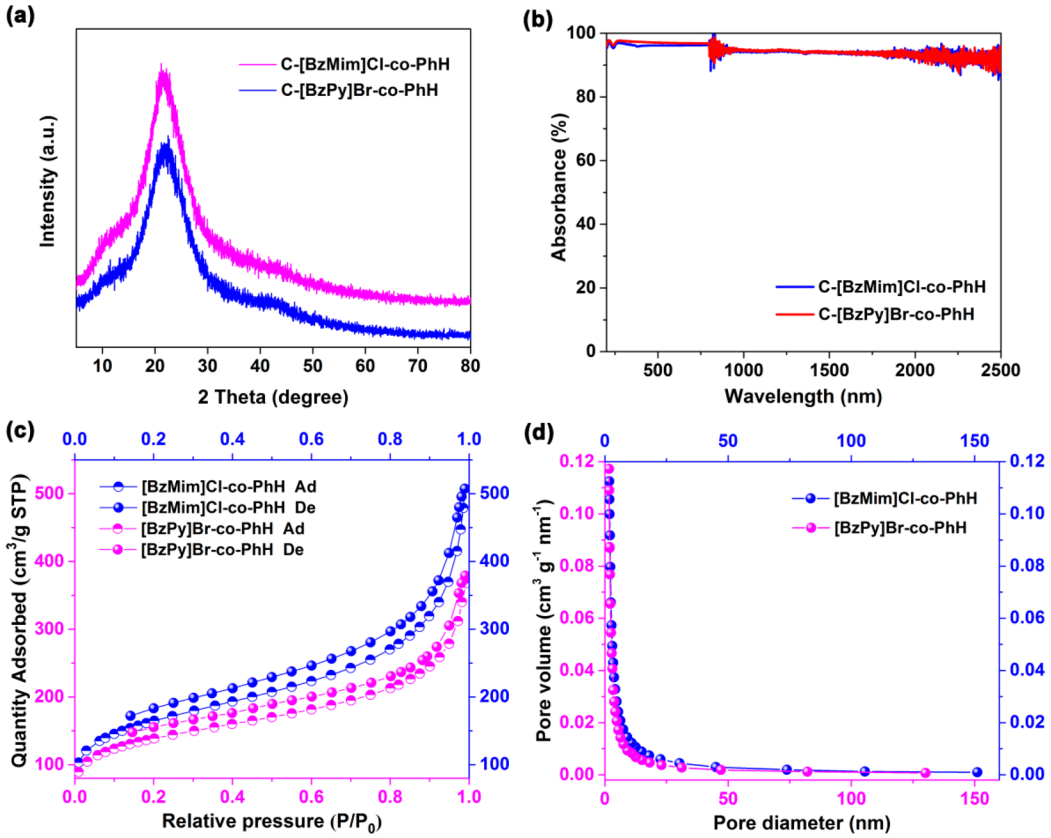

Figure 4. (a) XRD patterns of the C-[BzMim]Cl-*co*-PhH and C-[BzPy]Br-*co*-PhH. (b) Optical properties of the C-[BzMim]Cl-*co*-PhH and C-[BzPy]Br-*co*-PhH from 200 to 2500 nm. (c) N_2 adsorption/desorption isotherms of the C-[BzMim]Cl-*co*-PhH and C-[BzPy]Br-*co*-PhH. (d) Pore size distributions of the C-[BzMim]Cl-*co*-PhH and C-[BzPy]Br-*co*-PhH.

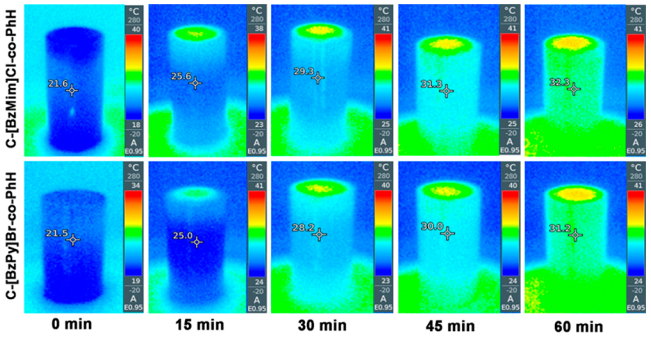

Figure 5. Infrared images of C-[BzMim]Cl-*co*-PhH and C-[BzPy]Br-*co*-PhH over irradiation time.

Supporting Information. The corresponding evaporation efficiencies of C-[BzMim]Cl-*co*-PhH are calculated to be 85.2%, 74.6%, and 71.3%, and for C-[BzPy]Br-*co*-PhH these values are 88.4%, 78.1%, and 73.6% under 1, 2, and 3 sun illumination intensities, respectively. Moreover, the evaporation efficiency of pure water is 22.6% under 1 sun illumination, which is much lower than that of C-[BzMim]Cl-*co*-PhH and C-[BzPy]Br-*co*-PhH at the same illumination intensity, indicating the C-[BzMim]Cl-*co*-PhH and C-[BzPy]Br-*co*-PhH have great potential to be efficient solar steam generations.

To confirm the stability of C-[BzMim]Cl-*co*-PhH and C-[BzPy]Br-*co*-PhH as solar steam generations, the cycle experiments were conducted 10 times under 1 sun illumination, and the resulting evaporation efficiencies are depicted in Figure 8a. The energy conversion efficiencies relatively remain unchanged within 10 cycles under 1 sun illumination, and the HCP samples keep their original appearance unchanged, indicating the C-[BzMim]Cl-*co*-PhH and C-[BzPy]Br-*co*-PhH possess excellent stability as solar steam devices. The artificial seawater with a salinity of 3.5% was prepared to evaluate the solar desalination performance of the C-[BzMim]Cl-*co*-PhH and C-[BzPy]Br-*co*-PhH under 1 sun illumination. The evaporation rates of C-[BzMim]Cl-*co*-PhH and C-[BzPy]Br-*co*-PhH for artificial seawater were calculated to be 1.27 and 1.38 kg m^{-2} h^{-1} under 1 sun illumination, respectively. In addition, a concentrated brine solution (with a salinity of 5, 10, and 15 wt %) was used to confirm the salt-resistance performance of the C-[BzMim]Cl-*co*-PhH and C-[BzPy]Br-*co*-PhH under 1 sun illumination. As shown in Figure S2c, with a salinity of 5, 10, and 15 wt % under 1 sun illumination, the evaporation rates of C-[BzMim]Cl-*co*-PhH were calculated to be 1.25, 1.21, and 1.19 kg m^{-2} h^{-1}, and for C-[BzPy]Br-*co*-PhH these values are 1.35, 1.32, and 1.29 kg m^{-2} h^{-1}, respectively. The evaporation rates slightly decrease with the increase of salinity, indicating the HCPs composites possess excellent salt resistance in solar steam generation. These results could be owed to porous structure and interconnected water channels, thus leading the pumped water replenish the surface vaporized water and avoid salt accumulation. The purified water was collected by water vapor condensation, and the concentrations of the metal ions (Na^+, Mg^{2+}, K^+, and Ca^{2+}) were measured by an atomic absorption spectrometer. As shown in Figure 8b, the concentration of Na^+, Mg^{2+}, K^+, and Ca^{2+} decreased significantly after desalination. The ion rejection rate is more

https://dx.doi.org/10.1021/acsaem.0c02290
ACS Appl. Energy Mater. 2020, 3, 11350−11358

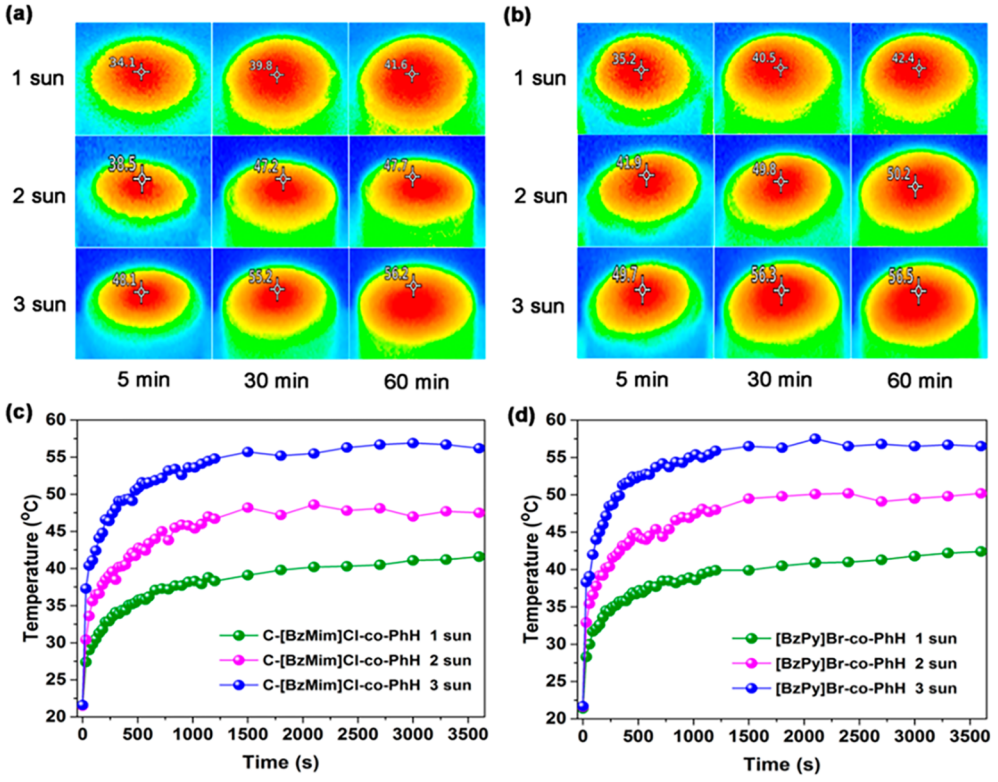

Figure 6. (a, b) Infrared images of the C-[BzMim]Cl-*co*-PhH and C-[BzPy]Br-*co*-PhH under different illuminations at different times. (c, d) Surface temperature changes of the C-[BzMim]Cl-*co*-PhH and C-[BzPy]Br-*co*-PhH under different illuminations.

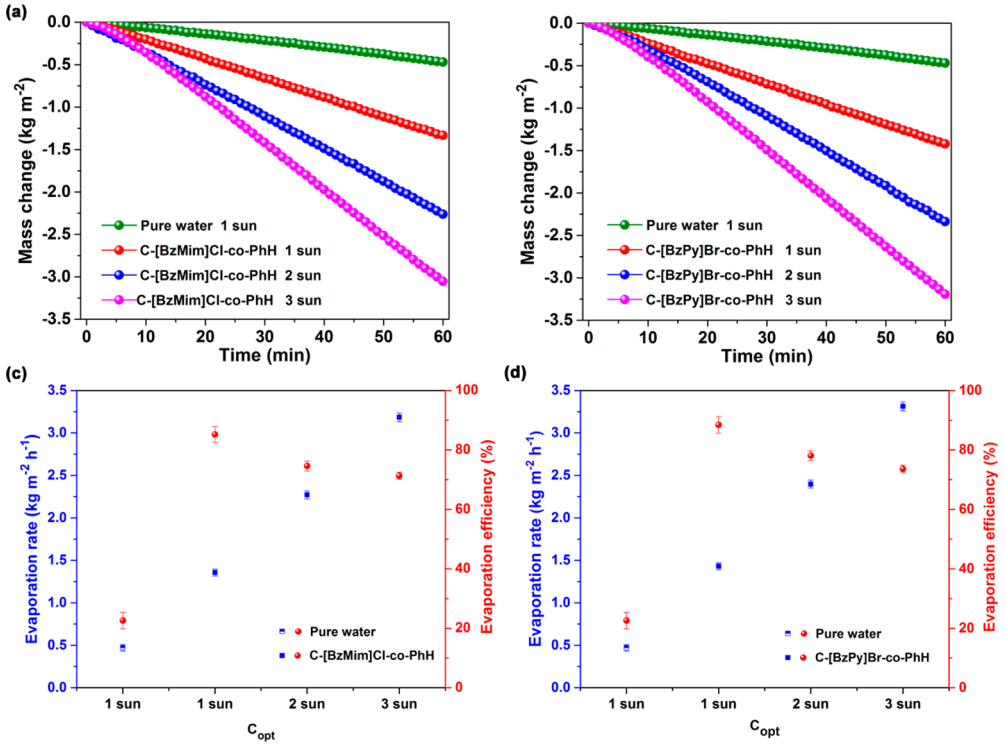

Figure 7. (a) Time-dependent mass changes of pure water and C-[BzMim]Cl-*co*-PhH under different illuminations. (b) Time-dependent mass changes of pure water and C-[BzPy]Br-*co*-PhH under different illuminations. (c) Evaporation rate and evaporation efficiency of pure water and C-[BzMim]Cl-*co*-PhH under different illuminations. (d) Evaporation rate and evaporation efficiency of pure water and C-[BzPy]Br-*co*-PhH under different illuminations.

than 99%; the concentration is much lower than the WHO's required standard for ion concentration of drinking water (Chinese National Standard GB5749-2006, World Health Organization and the US Environmental Protection Agency

https://dx.doi.org/10.1021/acsaem.0c02290
ACS Appl. Energy Mater. 2020, 3, 11350−11358

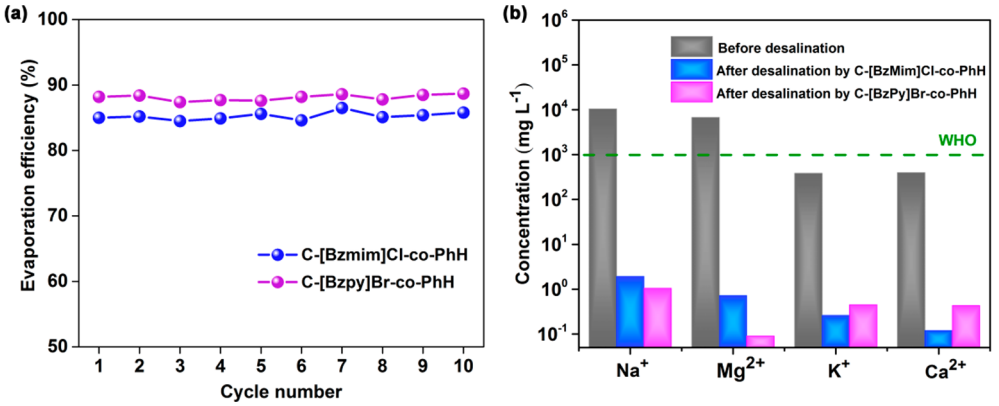

Figure 8. (a) Evaporation efficiency of the C-[BzMim]Cl-*co*-PhH and C-[BzPy]Br-*co*-PhH cycle for 10 times under 1 sun illumination. (b) Concentrations of four primary ions in artificial seawater before and after purification by using C-[BzMim]Cl-*co*-PhH and C-[BzPy]Br-*co*-PhH.

standards),[51] and the purified water can be used as domestic water directly, suggesting the potential applications of C-[BzMim]Cl-*co*-PhH and C-[BzPy]Br-*co*-PhH in solar desalination.

4. CONCLUSION

In summary, we have demonstrated a strategy for scalable fabrication of solar steam generation system based on hyper-cross-linked polymers (HCPs) by adding carbon black simultaneously. The prepared C-[BzMim]Cl-*co*-PhH and C-[BzPy]Br-*co*-PhH can serve as high-performance evaporators for solar water purification directly without any postprocessing. Based on the excellent properties including porous structure, excellent light absorption, and good thermal insulation, the C-[BzMim]Cl-*co*-PhH and C-[BzPy]Br-*co*-PhH show high photothermal conversion efficiencies of 85.2% and 88.4% under 1 sun illumination, respectively. Moreover, the C-[BzMim]Cl-*co*-PhH and C-[BzPy]Br-*co*-PhH as photothermal materials also exhibit good performance in solar desalination. The one-step synthesis strategy introduced in this work may offer a new avenue for the rational design and facile fabrication of the HCP based solar evaporators for efficient practical desalination.

■ ASSOCIATED CONTENT

Supporting Information

The Supporting Information is available free of charge at https://pubs.acs.org/doi/10.1021/acsaem.0c02290.

Characterizations; calculation of the energy conversion efficiency; the water contact angle of C-[BzMim]Cl-*co*-PhH and C-[BzPy]Br-*co*-PhH; and the salt-resistance performance of the C-[BzMim]Cl-*co*-PhH and C-[BzPy]Br-*co*-PhH (PDF)

■ AUTHOR INFORMATION

Corresponding Authors

Weidong Liang − *College of Petrochemical Technology, Lanzhou University of Technology, Lanzhou 730050, P. R. China*; Email: davidlucas@163.com

An Li − *College of Petrochemical Technology, Lanzhou University of Technology, Lanzhou 730050, P. R. China*; orcid.org/0000-0003-1982-1880; Email: lian2010@lut.cn

Authors

Chaohu Xiao − *College of Petrochemical Technology, Lanzhou University of Technology, Lanzhou 730050, P. R. China; College of Chemical Engineering, Experimental teaching department, Key Laboratory for Utility of Environment-friendly Composite Materials and Biomass in Universities of Gansu Province, Northwest Minzu University, Lanzhou 730030, P. R. China*

Qi-Meige Hasi − *College of Chemical Engineering, Experimental teaching department, Key Laboratory for Utility of Environment-friendly Composite Materials and Biomass in Universities of Gansu Province, Northwest Minzu University, Lanzhou 730030, P. R. China*

Fei Wang − *College of Petrochemical Technology, Lanzhou University of Technology, Lanzhou 730050, P. R. China*

Lihua Chen − *College of Chemical Engineering, Experimental teaching department, Key Laboratory for Utility of Environment-friendly Composite Materials and Biomass in Universities of Gansu Province, Northwest Minzu University, Lanzhou 730030, P. R. China*; orcid.org/0000-0002-2094-2279

Jingxian He − *College of Petrochemical Technology, Lanzhou University of Technology, Lanzhou 730050, P. R. China*

Fang Liu − *College of Petrochemical Technology, Lanzhou University of Technology, Lanzhou 730050, P. R. China*

Hanxue Sun − *College of Petrochemical Technology, Lanzhou University of Technology, Lanzhou 730050, P. R. China*

Zhaoqi Zhu − *College of Petrochemical Technology, Lanzhou University of Technology, Lanzhou 730050, P. R. China*

Complete contact information is available at: https://pubs.acs.org/10.1021/acsaem.0c02290

Notes

The authors declare no competing financial interest.

■ ACKNOWLEDGMENTS

The authors are grateful to the National Natural Science Foundation of China (Grants 21975113, 51663012, and 51962018), Project of Collaborative Innovation Team, Gansu Province, China (Grant 052005), Support Program for Hongliu Young Teachers of LUT, 2019 Key Talent Project of Gansu, and Innovation and Entrepreneurship Talent Project of Lanzhou (Grant 2017-RC-33).

REFERENCES

(1) Schiermeier, Q. Water risk as world warms. *Nature* **2014**, *505*, 10−11.

(2) Panwar, N. L.; Kaushik, S. C.; Kothari, S. Role of renewable energy sources in environmental protection: A review. *Renewable Sustainable Energy Rev.* **2011**, *15*, 1513−1524.

(3) Ni, G.; Zandavi, S. H.; Javid, S. M.; Boriskina, S. V.; Cooper, T. A.; Chen, G. A salt-rejecting floating solar still for low-cost desalination. *Energy Environ. Sci.* **2018**, *11*, 1510−1519.

(4) Han, Y.; Xu, Z.; Gao, C. Ultrathin Graphene Nanofiltration Membrane for Water Purification. *Adv. Funct. Mater.* **2013**, *23*, 3693−3700.

(5) Li, Q.; Chen, G. Q.; Liu, L.; Kentish, S. E. Spray Assisted Layer-by-Layer Assembled One-Bilayer Polyelectrolyte Reverse Osmosis Membranes. *J. Membr. Sci.* **2018**, *564*, 501−507.

(6) Lewis, N. S. Research opportunities to advance solar energy utilization. *Science* **2016**, *351*, aad1920.

(7) Zhu, L.; Gao, M.; Peh, C. K. N.; Ho, G. W. Solar-driven photothermal nanostructured materials designs and prerequisites for evaporation and catalysis applications. *Mater. Horiz.* **2018**, *5*, 323−343.

(8) Jiang, Q.; Tian, L.; Liu, K.; Tadepalli, S.; Raliya, R.; Biswas, P.; Naik, R. R.; Singamaneni, S. Bilayered Biofoam for Highly Efficient Solar Steam Generation. *Adv. Mater.* **2016**, *28*, 9400−9407.

(9) Zhu, L.; Gao, M.; Peh, C. K. N.; Ho, G. W. Recent Progress in Solar-driven Interfacial Water Evaporation: Advanced Designs and Applications. *Nano Energy* **2019**, *57*, 507−518.

(10) Storer, D. P.; Phelps, J. L.; Wu, X.; Owens, G.; Xu, H. Graphene and Rice Straw Fibre Based 3D Photothermal Aerogels for Highly Efficient Solar Evaporation. *ACS Appl. Mater. Interfaces* **2020**, *12*, 15279−15287.

(11) Li, Z.; Zhang, J.; Zang, S.; Yang, C.; Zhou, Y.; et al. Engineering controllable water transport of biosafety cuttlefish juice solar absorber toward remarkably enhanced solar-driven gas-liquid interfacial evaporation. *Nano Energy* **2020**, *73*, 104834.

(12) Zhou, X.; Lu, H.; Zhao, F.; Yu, G. Atmospheric Water Harvesting: A Review of Material and Structural Designs. *ACS Mater. Lett.* **2020**, *2*, 671−684.

(13) Chen, L.; Xia, M.; Du, J.; Luo, X.; Zhang, L.; Li, A. Superhydrophilic and Oleophobic Porous Architectures Based on Basalt Fibers as Oil-Repellent Photothermal Materials for Solar Steam Generation. *ChemSusChem* **2020**, *13*, 493−500.

(14) Li, X.; Xu, W.; Tang, M.; Zhou, L.; Zhu, B.; Zhu, S.; Zhu, J. Graphene oxide-based efficient and scalable solar desalination under one sun with a confined 2D water path. *Proc. Natl. Acad. Sci. U. S. A.* **2016**, *113*, 13953−13958.

(15) Wang, C.; Li, W.; Li, Z.; Fang, B. Solar thermal harvesting based on self-doped nanocermet: Structural merits, design strategies and applications. *Renewable Sustainable Energy Rev.* **2020**, *134*, 110277.

(16) Li, Z.; Wang, C.; Su, J.; Ling, S.; Wang, W.; An, M. Fast-Growing Field of Interfacial Solar Steam Generation: Evolutional Materials, Engineered Architectures, and Synergistic Applications. *Sol. RRL.* **2019**, *3*, 1800206.

(17) Ito, Y.; Tanabe, Y.; Han, J.; Fujita, T.; Tanigaki, K.; Chen, M. Multifunctional Porous Graphene for High-Efficiency Steam Generation by Heat Localization. *Adv. Mater.* **2015**, *27*, 4302−4307.

(18) Zhu, L.; Gao, M.; Peh, C. K. N.; Wang, X.; Ho, G. W. Self-Contained Monolithic Carbon Sponges for Solar-Driven Interfacial Water Evaporation Distillation and Electricity Generation. *Adv. Energy Mater.* **2018**, *8*, 1702149.

(19) Zhang, P.; Li, J.; Lv, L.; Zhao, Y.; Qu, L. Vertically Aligned Graphene Sheets Membrane for Highly Efficient Solar Thermal Generation of Clean Water. *ACS Nano* **2017**, *11*, 5087−5093.

(20) Li, Z.; Wang, C.; Lei, T.; Ma, H.; Su, J.; Ling, S.; Wang, W. Arched Bamboo Charcoal as Interfacial Solar Steam Generation Integrative Device with Enhanced Water Purification Capacity. *Adv. Sustainable Syst.* **2019**, *3*, 1800144.

(21) Kuang, Y.; Chen, C.; He, S.; Hitz, E.; Wang, Y.; Gan, W.; Mi, R.; Hu, L. A High-Performance Self-Regenerating Solar Evaporator for Continuous Water Desalination. *Adv. Mater.* **2019**, *31*, 1900498.

(22) Bian, Y.; Du, Q. Q.; Tang, K.; Shen, Y.; Hao, L. C.; Zhou, D.; et al. Carbonized Bamboos as Excellent 3D Solar Vapor-Generation Devices. *Adv. Mater. Technol.* **2019**, *4*, 1800593.

(23) Fang, J.; Liu, J.; Gu, J.; Liu, Q.; Zhang, W.; Su, H.; Zhang, D. Hierarchical Porous Carbonized Lotus Seedpods for Highly Efficient Solar Steam Generation. *Chem. Mater.* **2018**, *30*, 6217−6221.

(24) Yang, H. C.; Chen, Z.; Xie, Y.; Wang, J.; Elam, J. W.; Li, W.; Darling, S. B. Chinese Ink: A Powerful Photothermal Material for Solar Steam Generation. *Adv. Mater. Interfaces* **2019**, *6*, 1801252−1801258.

(25) Wang, Z.; Han, M.; He, F.; Peng, S.; Darling, S. B.; Li, Y. Versatile coating with multifunctional performance for solar steam generation. *Nano Energy* **2020**, *74*, 104886.

(26) Zhang, C.; Chen, Z.; Xia, Z.; Waldman, R. Z.; Wu, S. L.; Yang, H. C.; Darling, S. B. Ferric tannate photothermal material for efficient water distillation. *Environ. Sci.: Water Res. Technol.* **2020**, *6*, 911.

(27) Xia, Z. J.; Yang, H. C.; Chen, Z. W.; Waldman, R. Z.; Zhao, Y.; Zhang, C.; Patel, S. N.; Darling, S. B. Porphyrin Covalent Organic Framework (POF)-Based Interface Engineering for Solar Steam Generation. *Adv. Mater. Interfaces* **2019**, *6*, 1900254.

(28) Chen, Q.; Pei, Z.; Xu, Y.; Li, Z.; Yang, Y.; Wei, Y.; Ji, Y. A durable monolithic polymer foam for efficient solar steam generation. *Chem. Sci.* **2018**, *9*, 623−628.

(29) Zhu, Z.; Mu, P.; Fan, Y.; Bai, W.; Zhang, Z.; Sun, H.; Liang, W.; Li, A. Highly efficient solar steam generation of bilayered ultralight aerogels based on N-rich conjugated microporous polymers nanotubes. *Eur. Polym. J.* **2020**, *126*, 109560.

(30) Zhang, L.; Tang, B.; Wu, J.; Li, R.; Wang, P. Hydrophobic Light-to-Heat Conversion Membranes with Self-Healing Ability for Interfacial Solar Heating. *Adv. Mater.* **2015**, *27*, 4889−4894.

(31) Zhao, F.; Zhou, X.; Shi, Y.; Qian, X.; Alexander, M.; Zhao, X.; Mendez, S.; Yang, R.; Qu, L.; Yu, G. Highly efficient solar vapour generation via hierarchically nanostructured gels. *Nat. Nanotechnol.* **2018**, *13*, 489−495.

(32) Sun, Z.; Wang, J.; Wu, Q.; Wang, Z.; Wang, Z.; Sun, J.; Liu, C. J. Plasmon Based Double layer Hydrogel Device for a Highly Efficient Solar Vapor Generation. *Adv. Funct. Mater.* **2019**, *29*, 1901312.

(33) Tan, M.; Wang, J.; Song, W.; Fang, J.; Zhang, X. Self-floating hybrid hydrogels assembled with conducting polymer hollow spheres and silica aerogel microparticles for solar steam generation. *J. Mater. Chem. A* **2019**, *7*, 1244−1251.

(34) Zhou, Y.; Ding, T.; Gao, M.; Chan, K. H.; Cheng, Y.; He, J.; Ho, G. W. Controlled heterogeneous water distribution and evaporation towards enhanced photothermal water-electricity-hydrogen production. *Nano Energy* **2020**, *77*, 105102.

(35) Meng, F. L.; Gao, M.; Ding, T.; Yilmaz, G.; Ong, W. L.; Ho, G. W. Modular Deformable Steam Electricity Cogeneration System with Photothermal, Water, and Electrochemical Tunable Multilayers. *Adv. Funct. Mater.* **2020**, *30*, 2002867.

(36) He, J.; Zhang, Z.; Xiao, C.; Liu, F.; Sun, H.; Zhu, Z.; Liang, W.; Li, A. High-Performance Salt-Rejecting and Cost-Effective Superhydrophilic Porous Monolithic Polymer Foam for Solar Steam Generation. *ACS Appl. Mater. Interfaces* **2020**, *12*, 16308−16318.

(37) Xu, Y.; Jin, S.; Xu, H.; Nagai, A.; Jiang, D. Conjugated microporous polymers: design, synthesis and application. *Chem. Soc. Rev.* **2013**, *44*, 8012−8031.

(38) Liu, F.; Wang, S.; Lin, G.; Chen, S. Development and characterization of amine- functionalized hyper-cross-linked resin for CO_2 capture. *New J. Chem.* **2018**, *42*, 420−428.

(39) Mu, P.; Zhang, Z.; Bai, W.; He, J.; Sun, H.; Zhu, Z.; Liang, W.; Li, A. Superwetting Monolithic Hollow-Carbon-Nanotubes Aerogels with Hierarchically Nanoporous Structure for Efficient Solar Steam Generation. *Adv. Energy Mater.* **2019**, *9*, 1802158.

(40) Liu, F.; Liang, W.; Wang, C.; Xiao, C.; He, J.; Zhao, G.; Zhu, Z.; Sun, H.; Li, A. Superhydrophilic and mechanically robust phenolic

https://dx.doi.org/10.1021/acsaem.0c02290
ACS Appl. Energy Mater. 2020, 3, 11350−11358

resin as double layered photothermal materials for efficient solar steam generation. *Mater. Today Energy* **2020**, *16*, 100375.
(41) Mu, P. M.; Bai, W.; Zhang, Z.; He, J.; Sun, H.; Zhu, Z.; Liang, W.; Li, A. Robust aerogels based on conjugated microporous polymer nanotubes with exceptional mechanical strength for efficient solar steam generation. *J. Mater. Chem. A* **2018**, *6*, 18183−18190.
(42) Shan, X.; Chai, L.; Ma, J.; Qian, Z.; Chen, J.; Feng, H. B-doped carbon quantum dots as a sensitive fluorescence probe for hydrogen peroxide and glucose detection. *Analyst* **2014**, *139*, 2322−2325.
(43) Khachatryan, L.; Dellinger, B. Formation of chlorinated hydrocarbons from the reaction of chlorine atoms and activated carbon. *Chemosphere* **2003**, *52*, 709−716.
(44) Jheng, L.; Huang, C.; Hsu, S. L. ulfonated MWNT and imidazole functionalized MWNT/polybenzimidazole composite membranes for high-temperature proton exchange membrane fuel cell. *Int. J. Hydrogen Energy* **2013**, *38*, 1524−1534.
(45) Nasef, M. M.; Saidi, H.; Nor, H. M.; Yarmo, M. A. XPS studies of radiation grafted PTFE-g-polystyrene sulfonic acid membranes. *J. Appl. Polym. Sci.* **2000**, *76*, 336−349.
(46) He, J.; Zhao, G.; Mu, P.; Wei, H.; Su, Y.; Sun, H.; Zhu, Z.; Liang, W.; Li, A. Scalable fabrication of monolithic porous foam based on cross-linked aromatic polymers for efficient solar steam generation. *Sol. Energy Mater. Sol. Cells* **2019**, *201*, 110111.
(47) Liu, H.; Zhai, D. D.; Wang, M.; Liu, J. S.; Chen, X. Y.; Zhang, Z. J. Urea-Modified Phenol-Formaldehyde Resins for the Template-Assisted Synthesis of Nitrogen-Doped Carbon Nanosheets as Electrode Material for Supercapacitors. *ChemElectroChem.* **2019**, *6*, 885−891.
(48) Thommes, M.; Kaneko, K.; Neimark, A. V.; Olivier, J. P.; Rodriguez-Reinoso, F.; Rouquerol, J.; Sing, K. S. W. Physisorption of gases, with special reference to the evaluation of surface area and pore size distribution (IUPAC Technical Report). *Pure Appl. Chem.* **2015**, *87*, 1051−1069.
(49) Hong, S.; Shi, Y.; Li, R.; Zhang, C.; Jin, Y.; Wang, P. Nature-Inspired, 3D Origami Solar Steam Generator toward Near Full Utilization of Solar Energy. *ACS Appl. Mater. Interfaces* **2018**, *10*, 28517−28524.
(50) Li, X.; Ni, G.; Cooper, T.; Xu, N.; Li, J.; Zhou, L.; Hu, X.; Zhu, B.; Yao, P.; Zhu, J. Measuring Conversion Efficiency of Solar Vapor Generation. *Joule* **2019**, *3*, 1798−1803.
(51) Smith, A. H.; Lopipero, P. A.; Bates, M. N.; Steinmaus, C. M. Arsenic epidemiology and drinking water standards. *Science* **2002**, *296*, 2145−2146.

https://dx.doi.org/10.1021/acsaem.0c02290
ACS Appl. Energy Mater. 2020, 3, 11350−11358